Calcium Transport and Local Pool Regulate Polycystin-2 (TRPP2) Function in Human Syncytiotrophoblast

María del Rocío Cantero[†] and Horacio F. Cantiello[†‡*]
[†]Cátedra de Biofísica, Facultad de Odontología, Universidad de Buenos Aires, Buenos Aires, Argentina; and [‡]Massachusetts General Hospital East & Harvard Medical School, Charlestown, Massachusetts

ABSTRACT Polycystin-2 (PC2, TRPP2) is a Ca^{2+}-permeable, nonselective cation channel implicated in Ca^{2+} transport and epithelial cell signaling. Although PC2 may contribute to Ca^{2+} transport in human term placenta, the regulatory mechanisms associated with Ca^{2+} handling in this tissue are largely unknown. In this work we assessed the regulation by Ca^{2+} of PC2 channel function from a preparation of apical membranes of human syncytiotrophoblast ($PC2_{hst}$) reconstituted in a lipid bilayer system. Addition of either EGTA or BAPTA to the *cis* hemi-chamber, representing the cytoplasmic domain of the channel, and lowering Ca^{2+} to ~0.6–0.8 nM, inhibited spontaneous $PC2_{hst}$ channel activity, with a time response dependent on the chelator tested. EGTA reduced $PC2_{hst}$ channel currents by 86%, with a $t_{1/2} = 3.6$ min, whereas BAPTA rapidly and completely (100%) eliminated channel activity with a $t_{1/2} = 0.8$ min. Subsequent titration with Ca^{2+} reversed the inhibition, which followed a Hill-type function with apparent dissociation constants of 1–5 nM, and 4 Ca^{2+} binding sites. The degree of inhibition by the *cis* Ca^{2+} chelator largely depended on increasing *trans* Ca^{2+}. This was consistent with measurable Ca^{2+} transport through the channel, feeding the regulatory sites in the cytoplasmic domain. Interestingly, the reconstituted in vitro translated PC2 ($PC2_{iv}$) was completely insensitive to Ca^{2+} regulation, suggesting that the regulatory sites are not intrinsic to the channel protein. Our findings demonstrate the presence of a Ca^{2+} microdomain largely accessible through the channel that controls PC2 function in human syncytiotrophoblast of term placenta.

INTRODUCTION

The human syncytiotrophoblast (hST) transfers Ca^{2+} from mother to the fetus, to meet developmental needs, particularly during the third trimester of pregnancy (1,2). Ca^{2+} entry by the hST is thought to be mediated by ion channels, whose molecular identity remains to be fully determined. A number of Ca^{2+}-permeable ion channels present in human placenta may contribute to this function, including L-type and T-type voltage-gated channels, and the highly Ca^{2+} permeable TRP channel isotypes TRPV5 and TRPV6 (3–6). Limited information is presently available, however, regarding the possible contribution of these channels to Ca^{2+} transport in the placenta. Studies from our laboratory determined the abundant expression of another TRP isotype, polycystin-2 (PC2, TRPP2), in the hST of term placenta (7). PC2 is the product of the gene *PKD2*, whose mutations cause autosomal dominant polycystic kidney disease (ADPKD) (8). PC2 may be relevant to epithelial Ca^{2+} transport due to its large nonselective cation conductance and slight selectivity to divalent cations (7).

PC2 is expressed in various epithelial tissues and other organs, where it is largely associated with Ca^{2+} transport and cell activation (9,10). This channel protein is found in several cell locations, including the primary cilium, intracellular Ca^{2+} stores, and the plasma membrane (10,11). PC2 shares homology with voltage-gated Na^{+}, and Ca^{2+} channels (8), both in the pore region, and in putative Ca^{2+}-binding domains such as the EF-hand (8,12), that may contribute to Ca^{2+}-dependent channel regulation (13,14). Cytoplasmic Ca^{2+} regulation of PC2 function in the plasma membrane may entail direct interactions with the channel protein. Vassilev et al. (15) reported the transient activation of wild-type PC2 by increasing the intracellular Ca^{2+} concentration from 0.1 to 1 μM in *Xenopus laevis* oocytes overexpressing the protein. This regulation was absent in the truncated PC2 carrying the mutation R742X, which lacks the cytoplasmic terminus, and causes ADPKD. Cai et al. (16) determined that wild-type PC2 Ca^{2+}-dependent, bell-shaped open probability in response to voltage shifts in the mutated PC2-S812A carrying an alanine substitution in Ser^{812}, which represents a casein kinase phosphorylation site. Previous studies from our laboratory demonstrated that intracellular Ca^{2+} regulation of PC2 function in the hST implicates interactions with the actin cytoskeleton and actin-associated proteins. The PC2 stimulatory effect of the actin filament disrupter cytochalasin D in reconstituted hST apical membranes was mimicked by addition of gelsolin from the *cis* (cytoplasmic) site of the reconstitution chamber in the presence, but not the absence, of micromolar Ca^{2+} (17). Thus, Ca^{2+} regulation of PC2 may implicate diverse mechanisms, entailing both the channel itself and/or regulatory proteins associated with it.

Herein, we explored the response to Ca^{2+} of $PC2_{hst}$ from reconstituted hST apical membranes and the in vitro translated PC2 ($PC2_{iv}$) after addition of Ca^{2+} chelators EGTA and BAPTA. Whereas $PC2_{iv}$ was insensitive to changes in Ca^{2+} concentrations, $PC2_{hst}$ activity decreased to different

Submitted February 27, 2013, and accepted for publication May 30, 2013.
*Correspondence: hcantiello@yahoo.com.ar
Editor: Randall Rasmusson.

0006-3495/13/07/0365/11 $2.00
http://dx.doi.org/10.1016/j.bpj.2013.05.058

degrees and kinetics responses depending on the chelator, and the *trans* Ca^{2+} concentration. The evidence suggested the presence of cooperative Ca^{2+} binding sites, which are not intrinsic to, but regulate, $PC2_{hst}$. The evidence supports a feedback mechanism of a local cytoplasmic Ca^{2+} pool, with intracellular high-affinity Ca^{2+} binding sites, which are in turn modulated by Ca^{2+} entry through the channel in hST.

MATERIALS AND METHODS

Human placenta membrane preparation

Apical hST plasma membranes from term human placenta were obtained as previously described in González-Perrett et al. (7). Briefly, normal placenta from vaginal deliveries were obtained and immediately processed. The villous tissue was fragmented, washed with ice-cold unbuffered NaCl saline (150 mM), and minced into small pieces. The fragmented tissue was processed, filtered, and centrifuged, as previously reported in González-Perrett et al. (7). The final pellet was resuspended in a buffer solution containing HEPES 10 mM, sucrose 250 mM, and KCl 20 mM and adjusted to pH 7.4, and was then aliquoted and stored frozen until the time of the experiment. Apical hST enrichment usually was higher than 26-fold.

Preparation of in vitro translated PC2

In vitro translated PC2 ($PC2_{iv}$) was prepared as previously reported in González-Perrett et al. (7), with a reticulocyte lysate system TnT T7 (Promega, Fitchburg, WI). The plasmid pGEM-PKD2 encoding PC2, was in vitro transcribed and translated with a reticulocyte lysate system TnT T7 (Promega) by incubation of plasmid DNA (1 μg) and 50 μL of the reaction mixture for 90 min at 30°C. The $PC2_{iv}$ was introduced by dialysis into liposomes as previously reported in González-Perrett et al. (7).

Ion channel reconstitution

PC2 containing vesicles were reconstituted into lipid bilayers as previously reported in González-Perrett et al. (7) in a KCl chemical gradient (*cis*/*trans*, 150:15 mM). PC2 containing vesicles were incorporated into lipid bilayers of a reconstitution system. The lipid mixture was a 7:3 ratio of POPC and POPE (20–25 mg/mL; Avanti Polar Lipids, Birmingham, AL) in *n*-decane. Unless otherwise stated, the *cis* chamber contained a solution of KCl 150 mM, $CaCl_2$ 10 μM, and HEPES 10 mM, at pH 7.40. The *trans* side contained a similar solution with lower KCl (15 mM), to create a KCl chemical gradient. $PC2_{hst}$ was identified as previously reported in González-Perrett et al. (7), by a large conductance (~170 pS), K^+-conducting channel, which was inhibited by *trans* (external) amiloride, and *cis* (cytoplasmic side of PC2) anti-PC2 antibody, properties that also ensured its orientation in the reconstituted membrane (7).

Reagents and Ca^{2+} chelation

EGTA was dissolved in NaOH and titrated with HCl to reach pH 7.1. BAPTA was dissolved in dimethylsulfoxide. The concentrated reagents (16 μL and 8 μL, respectively) were diluted in either *cis* (1600 μL) or *trans* (1000 μL) chambers and buffered at pH 7.4 (10 mM HEPES), to reach final concentrations of 1 mM and 2 mM, respectively (see Results). Neither chelator nor vehicle alone affected the final pH. The Ca^{2+} concentration was calculated by

$$[\mathrm{Ca}] = \frac{K_Q[\mathrm{Ca}Q]}{[Q]}, \quad (1)$$

where K_Q, is the dissociation constant of the Ca^{2+}-chelator complex, $[Q]$ is the concentration of the free chelating agent, and $[CaQ]$ is the concentration of Ca^{2+} bound to Q. The final free Ca^{2+} concentration was estimated to be either 0.6 or 0.8 nM (pH ~7.4) in the presence of EGTA or BAPTA, respectively (more details in the Supporting Material).

Data acquisition and analysis

Single channel currents obtained at 40–60 mV with a PC501A patch-clamp amplifier (Warner Instruments, Hamden, CT) with a 10 gigaOhm feedback resistor and signal were driven and processed with the software pCLAMP 6.2 (7). Output (voltage) signals were low-pass-filtered at 700 Hz (3 dB) with an eight-pole, Bessel-type filter (Frequency Devices, Haverhill, MA). Single channel current tracings were further filtered for display purposes only. Unless otherwise stated, the software pCLAMP, Ver. 10.0 (Axon Instruments, Foster City, CA), was used for data analysis and the software SIGMAPLOT, Ver. 11.0 (Jandel Scientific, Corte Madera, CA), was used for statistical analysis and graphics. Unless otherwise stated, all tracings shown in this study were obtained at holding potentials between 40 and 60 mV. PC2 channel identification was conducted as previously reported in González-Perrett et al. (7). Statistical significance was obtained by unpaired Student's *t*-test comparison of sample groups of similar size, and accepted at $p < 0.05$. Average data values were expressed as the mean ± SE (N) under each condition, where n represents the total number of experiments analyzed.

RESULTS

Effect of Ca^{2+} chelation on $PC2_{hst}$ channel function

To assess the effect of cytoplasmic Ca^{2+} on $PC2_{hst}$ channel function, hST apical vesicles were reconstituted in the presence of a KCl chemical gradient, (150 mM KCl in *cis*, and 15 mM *trans*), with symmetrical Ca^{2+} (10 μM), and pH 7.4 (Fig. 1 *a*, Ctrl). Once spontaneous channel activity was observed, EGTA (1 mM) was added to the *cis* chamber to reduce the free Ca^{2+} concentration to ~0.6 nM. Ca^{2+} chelation decreased the $PC2_{hst}$-mediated K^+ mean currents by 86% (6.25 ± 1.8 vs. 0.88 ± 0.08 pA, $N = 24$, $p < 0.05$) with a $t_{1/2}$ of 3.6 min (Fig. 1, *a* and *c*). The EGTA inhibition was never complete, leaving a remainder current (~14%, Fig. 1 *c*). A lag in the response was usually observed, before a decrease in current was noticeable after EGTA addition (Fig. 1 *c*). The inhibitory effect of lowering *cis* Ca^{2+} on $PC2_{hst}$ channel function was confirmed with another Ca^{2+}-chelating agent, BAPTA (2 mM), which produced a faster ($t_{1/2} = 0.4$ min) and complete (100%, $N = 8$) inhibition of channel function (Fig. 1 *c*). It is important to note that higher concentrations of EGTA never reproduced the effect of BAPTA, nor achieved complete inhibition but instead generated membrane instability (data not shown). Thus, only 1 mM EGTA data are reported herein.

Effect of *cis* Ca^{2+} chelation on $PC2_{iv}$ channel activity

The above results indicated the presence of Ca^{2+} regulatory sites in $PC2_{hst}$ that control its function. Thus, $PC2_{iv}$ was also

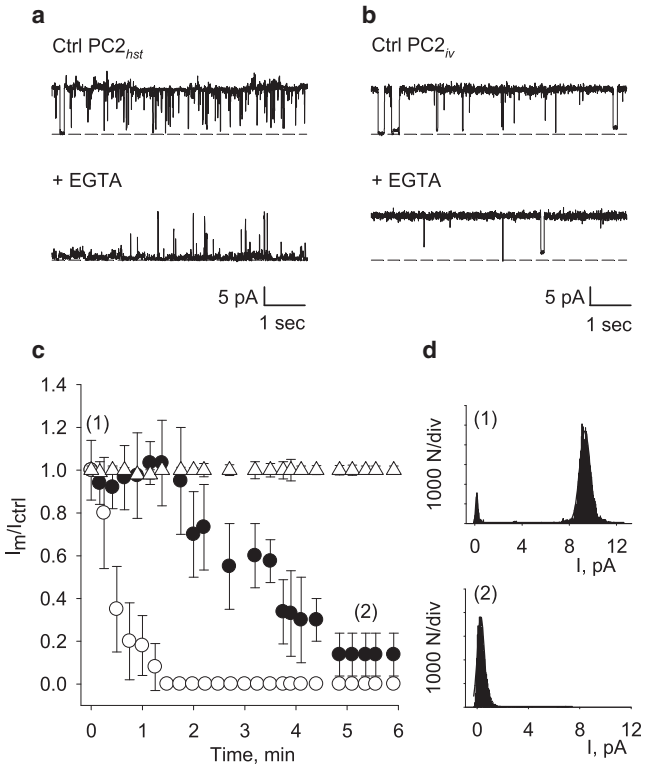

FIGURE 1 Effect of Ca^{2+} chelation on PC2 channel function. (*a*) Representative single channel tracings of reconstituted $PC2_{hst}$. Addition of *cis* EGTA (1 mM) inhibited channel function after 5 min ($N = 24$). (*b*) Representative single channel tracings of reconstituted $PC2_{iv}$ as in panel *a*. Addition of EGTA (1 mM) to the *cis* chamber had no effect on channel function ($N = 5$). (*c*) Relative current (I_m/I_{ctrl}) after addition of either EGTA (1 mM, *solid circles*) or BAPTA (2 mM, *open circles*) to $PC2_{hst}$ and EGTA (1 mM, *triangles*) to $PC2_{iv}$. Experimental data are the mean ± SE of 24, 8, and 5 experiments, respectively. (*d*) All-point histograms of single channel tracings from panel *a*.

reconstituted in a lipid bilayer system. Spontaneous $PC2_{iv}$ single channel currents were neither modified by addition of EGTA (1 mM) to the *cis* side (8.1 ± 0.4 pA vs. 8.2 ± 0.3 pA, $N = 5$, Fig. 1, *b* and *c*) nor by BAPTA (2 mM) (data not shown). Actually, the $PC2_{iv}$ protein did not respond to high Ca^{2+} in the *trans* compartment either (see Table S1 in the Supporting Material). Thus, in contrast to $PC2_{hst}$, Ca^{2+} chelation did not affect single channel currents through the $PC2_{iv}$ isolated protein.

$PC2_{hst}$ function recovery by Ca^{2+} addition to the *cis* chamber

To determine whether the inhibition of $PC2_{hst}$ by Ca^{2+} chelation was reversible, the *cis* chamber was titrated with increasing concentrations of Ca^{2+} in the presence of chelator (Fig. 2 *a*). The *cis* free Ca^{2+} was correlated with the recovery of $PC2_{hst}$ channel function that was obtained as fractional currents after either EGTA or BAPTA conditions (Fig. 2, *a* and *b*). Inhibition from either chelator was entirely reversible. Mean recovery data as a function of $[Ca^{2+}]_{cis}$ for both chelating agents were best fitted with a Hill-type equation (18) (Fig. 2 *b*) that followed

$$\frac{I_m}{I_{\max}} = \frac{[\mathrm{Ca}]^{n_H}}{[\mathrm{Ca}]^{n_H} + K_D^{n_H}} + I_b, \qquad (2)$$

where K_D is the Ca^{2+} apparent dissociation constant for the binding sites associated with the n_H, namely the Hill coefficient, and I_b and $I_{\max}$ are the basal (Ca^{2+} insensitive) and maximal currents, respectively. The results showed a $K_D = 5.01 \pm 0.06$ nM ($I_b = 0.08$, $n_H = 4.0 \pm 0.3$) in the presence of EGTA, and a $K_D = 1.75 \pm 0.13$ nM ($I_b = 0.04$, $n_H = 4.0 \pm 0.2$) in the presence of BAPTA (Fig. 2 *b*). These results suggested the presence of at least four regulatory Ca^{2+} binding sites of $PC2_{hst}$ channel function, although n_H does not represent the actual number of binding sites. In its simplified form, the Hill equation describes an allosteric interaction between originally identical, unoccupied binding sites (18,19). Changes in affinity occur as these sites become increasingly occupied. Thus, n_H is, strictly

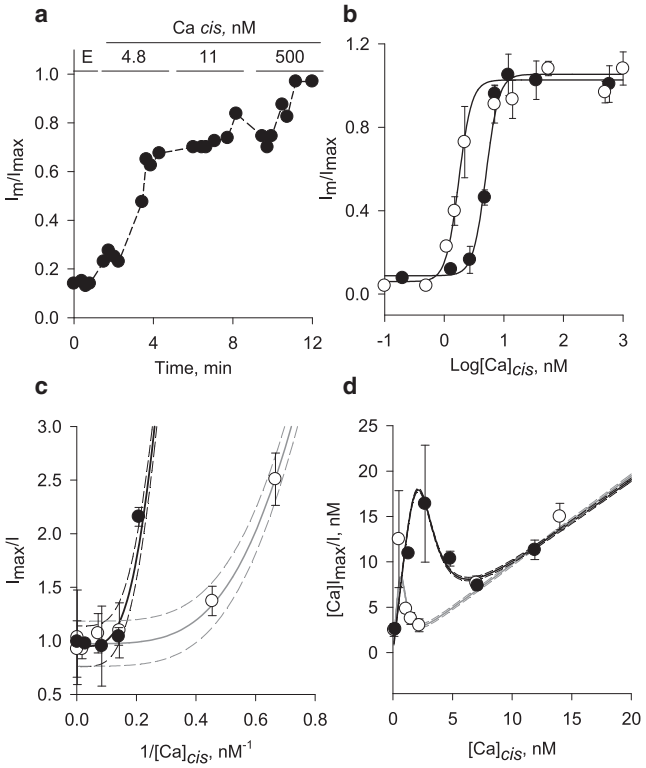

FIGURE 2 Recovery by Ca^{2+} of $PC2_{hst}$ channel function after Ca^{2+} chelation. (*a*) Time response of current change after addition of different Ca^{2+} concentrations to the *cis* chamber after inhibition by EGTA. (*b*) Recovery curves as a function of *cis* Ca^{2+} concentration, after addition of either EGTA (*solid circles*) or BAPTA (*open circles*). Experimental data are the mean ± SE of seven and five experiments, respectively. (*Solid lines*) Best fitted Hill-type equation. Scatchard (*c*), and Hanes (*d*) plots of fitted EGTA (*black line*) and BAPTA (*shaded line*) recovery curves. (*Dashed lines*) Mean ± SE of fitted results.

speaking, a measurement of cooperation, not of the actual number of binding sites (or their intrinsic binding affinity). The simplified Hill equation will have an n_H, which will only represent the actual number of binding sites, as positive cooperativity becomes very strong ($n_H \rightarrow n$). Strong cooperation was suggested by the nonlinear Scatchard and Hanes plots (Fig. 2, *c* and *d*) and calculation of R_s which, as defined by Bisswanger (19), is the ratio of ligand concentration at 90 and 10% saturation, respectively, with a value of 81 for a normal hyperbolic saturation curve. The value R_s decreases with the strength of positive cooperativity. We defined R_s as the ratio between 90 and 10% saturation values from the titration curves, respectively (18,19). The R_s values, 4.31 and 3.44 obtained after recovery from EGTA and BAPTA inhibition, respectively, were in agreement with a strong positive cooperativity ($R_s << 81$ (18,19)).

We further evaluated an expanded Hill equation considering that if ligand binding cooperativity is very marked, then the fraction of all channel-ligand states containing fewer than n molecules of ligand would be negligible at any concentration that is appreciable compared to the intrinsic constant, K_s (18). In such cases, the Hill equation may be rewritten with the assumption that $n_H = 4$, such that

$$\frac{I}{I_{\max}} = \frac{[\mathrm{Ca}]^4}{[\mathrm{Ca}]^4 + a^3b^2cK_s^4} + I_b, \tag{3}$$

where a, b, and c are factors by which the intrinsic binding constants have been increased in each step, and $a^3b^2cK_s{}^4 = K_D{}^4$, in Eq. 3. The parameters obtained from the recovery dose-response fitted data to Eq. 3 are shown in Table S2, where the highest dissociation constant for the first binding site of either EGTA or BAPTA conditions were 111.6 and 105 nM, respectively.

Diffusional limitation corrections

Although Ca^{2+} binding interactions to the putative binding sites after recovery from inhibition by either chelator were almost identical (see Table S2), current decay (Fig. 1 *c*) was faster and stronger in the presence of BAPTA as compared with EGTA (7:1). This difference could not be explained by either binding interaction or by the forward rate constants of the chelators, which relate as 100:1 (20). Thus, we explored the possibility that a diffusional limitation of the chelators could be limited to the Ca^{2+} binding sites. Thus, we corrected the recovery curves by a transport coefficient (h) ((19), also see the Supporting Material), considering the diffusive properties of EGTA and BAPTA (20,21). This coefficient represented the existence of a diffusional layer between the channel and bulk Ca^{2+}, which would have distinct diffusive properties for either chelator. Under these conditions, diffusional Ca^{2+} flow (J_{diff}) from the bulk solution (C_2) to the diffusional limitation layer (C_1) would be described as

$$J_{\mathrm{diff}} = h([C_2] - [C_1]) = \frac{D_C([C_2] - [C_1])}{\delta}, \tag{4}$$

where δ represents the layer thickness, and D_C the diffusion constant of the chelating agent (20). Once Ca^{2+} accesses the regulatory sites, $PC2_{hst}$ activation will follow the function described by Hill (Eq. 2). Under steady-state conditions, J_{diff} and the activation process would occur at the same velocity (19), such that

$$h([C_2] - [C_1]) = \frac{V[C_1]^n}{K_D^n + [C_1]^n}. \tag{5}$$

To estimate h, we plotted $I_m/I_{\max}$ versus time after Ca^{2+} addition to the *cis* chamber following either EGTA or BAPTA inhibition, respectively (see Fig. S1 *a* in the Supporting Material). The slopes of the curves were plotted versus the *cis* Ca^{2+} concentration (see Fig. S1 *b*). The transport coefficients obtained, $4.3 \pm 1.3 \times 10^{-3}$ s^{-1} nM^{-1} ($r = 0.82$) and $2.5 \pm 1.7 \times 10^{-3}$ s^{-1} nM^{-1} ($r = 0.58$) for EGTA and BAPTA, respectively, were not statistically different from each other ($p > 0.05$), indicating that the two chelators did not display any relevant diffusional differences. Even further correction taking into account the actual diffusional coefficient ratio of the chelators ($D_{\mathrm{EGTA}}/D_{\mathrm{BAPTA}} = 1.1$), based on their difference in molecular size (molecular mass 380.35 vs. 476.43 g/mol for EGTA and BAPTA, respectively), did not render further differences, but actually favored slightly EGTA over BAPTA (data not shown). These coefficients were corrected considering that Ca^{2+} was added at an average distance (d) of 500 μm from Ca^{2+} regulatory sites (approximately center of the cuvette), and h could then be calculated as

$$h = m_i\ d, \tag{6}$$

where i represents either chelator.

The h values obtained were 2.15 $\mu m\ s^{-1}$ and 1.25 $\mu m\ s^{-1}$, for EGTA and BAPTA, respectively. The corrected $PC2_{hst}$ reactivation curves (see Fig. S1 *c*), following Bisswanger (19), showed a left shift in the corrected K_D (K_D') that was greater in the case of EGTA than of BAPTA, with corrected values of 4.70 ± 0.02 nM ($n_H = 4.1 \pm 0.07$), and a K_D of 1.26 ± 0.03 nM ($n_H = 4.5 \pm 0.04$) for Ca^{2+}, respectively. Thus, the values fell within the experimental error, such that the diffusional contribution would be negligible for either chelator.

Effect of external Ca^{2+} on $PC2_{hst}$ channel function

To explore whether external Ca^{2+} also had an effect on $PC2_{hst}$ channel function, we increased the Ca^{2+} concentration from the *trans* side after channel inhibition with EGTA. A rise in *trans* Ca^{2+} rapidly increased $PC2_{hst}$

channel function, which reached a peak current higher (240%) than control (before EGTA addition) at ~5 mM Ca^{2+} (Fig. 3 *a*). Further addition of external Ca^{2+} (10–50 mM $CaCl_2$) decreased the mean currents through $PC2_{hst}$. In the presence of *cis* BAPTA, however, increasing concentrations of *trans* Ca^{2+} did not restore $PC2_{hst}$ channel function (Fig. 3 *b*). These findings raised the hypothesis that the differences in inhibition elicited by either chelator may be associated with a remainder channel function, as in the case of EGTA, which should drive Ca^{2+} through, from the *trans* compartment. This was explored in the next section.

Effect of Ca^{2+} chelation at different initial *trans* Ca^{2+} concentrations

To further explore the changes observed in $PC2_{hst}$ channel function by titration of external Ca^{2+}, experiments were also designed to test the effect of the *cis* chelator at a given initial *trans* Ca^{2+} concentration. The experiment was initiated with a given *trans* Ca^{2+} already present in the chamber before addition of the *cis* chelator. In the presence of low external Ca^{2+} (0.6 nM), addition of EGTA (Fig. 4 *a*) elicited a rapid and almost complete inhibition with $t_{1/2} = 0.4$ min, which was rather similar to the BAPTA effect with 10 μM Ca^{2+} *trans*. Conversely, in the presence of high (1 mM) external Ca^{2+}, *cis* EGTA only had a transient and incomplete effect, reaching 50% inhibition (Fig. 4 *a*). Because the BAPTA effect was fast and complete in symmetrical 10 μM Ca^{2+}, we also tested the effect of BAPTA while in the presence of high (1 mM) *trans* Ca^{2+}, which only elicited a transient inhibition of the currents by 20%, returning to control values in ~1 min (Fig. 4 *b*). Thus, the inhibitory

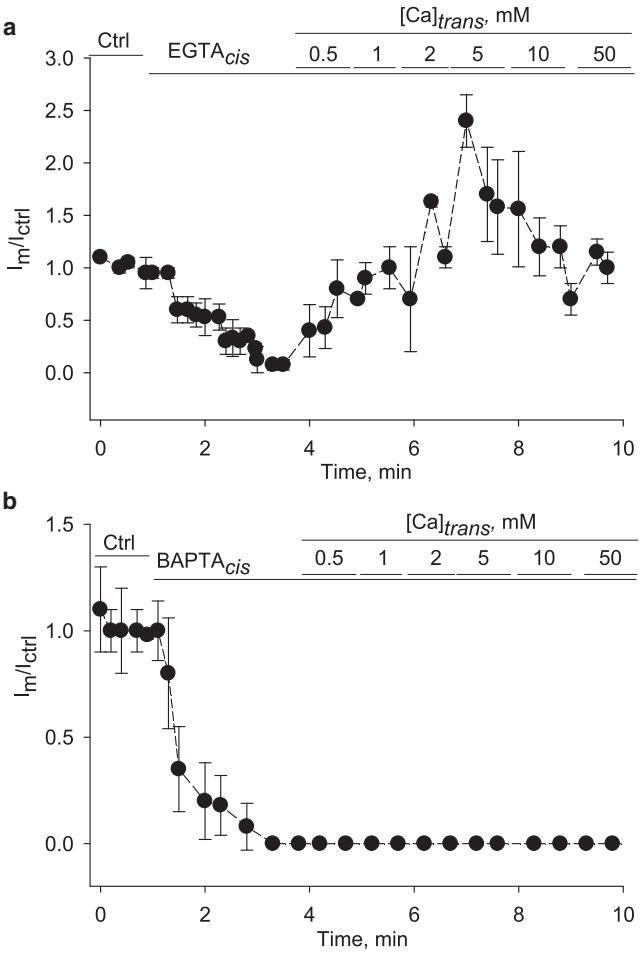

FIGURE 3 Effect of *trans* Ca^{2+} on $PC2_{hst}$ function. (*a*) Kinetics of the I_m/I_{ctrl} ratio under control conditions (*Ctrl*), after *cis* EGTA addition, followed by increasing Ca^{2+} concentrations added to the *trans* side. Experimental data (*solid circles*) are the mean ± SE ($N = 5$). (*b*) Similar data as in panel *a*, after addition of BAPTA. Experimental data (*solid circles*) are the mean ± SE ($N = 3$).

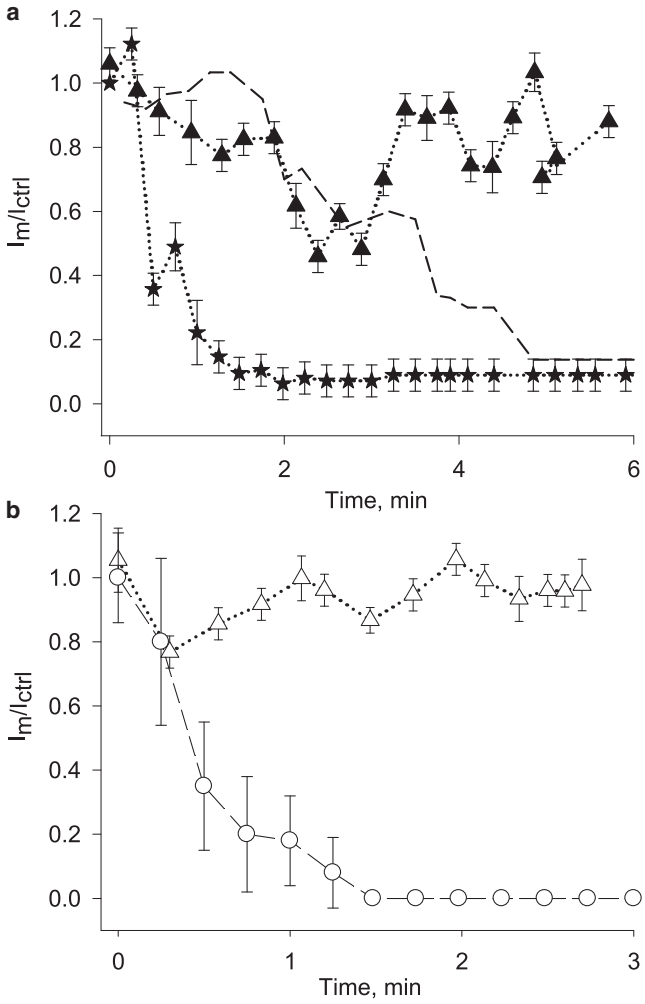

FIGURE 4 Effect of *trans* Ca^{2+} on $PC2_{hst}$ channel inhibition. (*a*) Kinetics of channel recovery (I_m/I_{ctrl}) after EGTA addition at different initial *trans* Ca^{2+} concentrations. Experimental data were obtained in 1 mM (*triangles*) and 0.6 nM (*stars*) Ca^{2+} conditions, respectively. Experimental data are expressed as mean ± SE ($N = 3$). (*b*) Kinetics of channel recovery (I_m/I_{ctrl}) after BAPTA addition in the presence of 1 mM *trans* Ca^{2+} concentration (*triangles*). Experimental data are expressed as mean ± SE ($N = 3$). (*Dashed lines*) Values obtained in the presence of 10 μM *trans* Ca^{2+} (Fig. 1 *c*).

effect of *cis* Ca^{2+} chelation (with either chelator) on $PC2_{hst}$ channel function strongly depended on the *trans* Ca^{2+} concentration. This would suggest that the Ca^{2+} chemical gradient, and thus permeation through the channel pore, modifies the availability of Ca^{2+} in the proximity to the regulatory sites in the *cis* compartment.

Calculation of Ca^{2+} flux coefficient through $PC2_{hst}$

The results obtained in the presence of different *trans* Ca^{2+} concentrations allowed us to determine the contribution $PC2_{hst}$ made to Ca^{2+} transport and its delivery to the *cis* side. Ca^{2+} transport through the channel was calculated as the rate of $PC2_{hst}$ channel recovery. To this end, we increased the *trans* Ca^{2+} concentration after *cis* EGTA channel inhibition, and then obtained the fractional recovery current I_m/I_{max} as a function of $[Ca^{2+}]_{trans}$ (Fig. 5 *a*, *left*). The relationship was well approximated by a Michaelis-Menten-type function with an apparent dissociation constant of 2.8 ± 0.92 mM and $n = 1.0 \pm 0.4$. The relationship $t_{1/2}$ versus $[Ca^{2+}]_{trans}$ evidenced a linear function (Fig. 5 *b*).

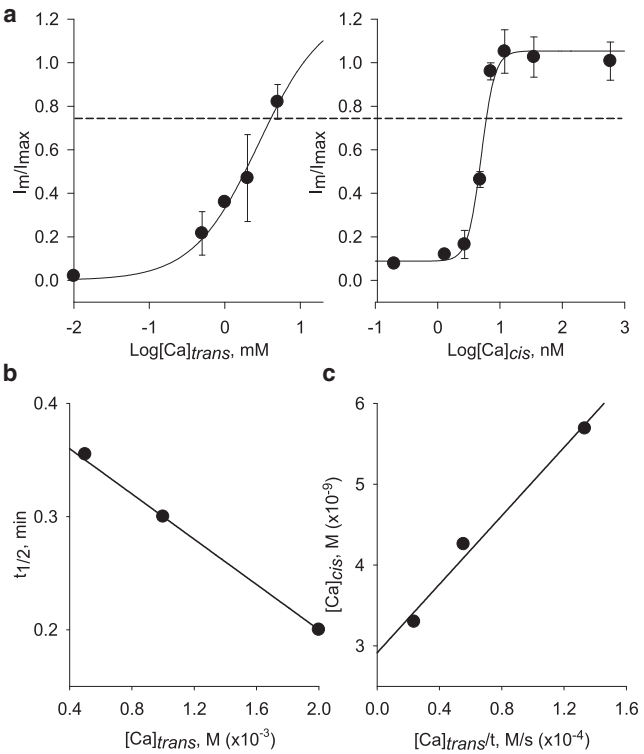

FIGURE 5 Recovery of $PC2_{hst}$ channel activity by either *cis* or *trans* Ca^{2+}. (*a*) (*Left*) $PC2_{hst}$ function (I_m/I_{max}) recovery curve in the presence of increasing *trans* Ca^{2+} concentrations. (*Right*) Recovery curve in the presence of increasing *cis* Ca^{2+} concentrations (from Fig. 2 *b*). (*Dashed line*) $I_m/I_{max} = 0.75$ reached in both graphs. (*b*) Experimental $t_{1/2}$ as a function of *trans* Ca^{2+} concentration. The curve was fitted with $t_{1/2} = m\,[Ca^{2+}]_{trans} + t_0$, where $m = -100$ min.M^{-1} and $t_0 = 0.40$ min. (*c*) Correlation between *cis* and *trans* Ca^{2+} concentrations generating similar I_m/I_{max} ratios.

Because the results with *cis* Ca^{2+} titration indicated that the regulatory effect of Ca^{2+} on $PC2_{hst}$ was only possible from the *cis* side, we compared the I_m/I_{max} for both $[Ca^{2+}]_{trans}$ and $[Ca^{2+}]_{cis}$ titrations, thus obtaining the ratio between *trans* and *cis* Ca^{2+} to reach similar recovery values (i.e., Fig. 5 *a*, *dashed line*). This recovery ratio was thus associated with a Ca^{2+} influx (J_{Ca}) for each *trans* Ca^{2+} concentration. Further, the *trans* Ca^{2+} concentration was inversely correlated with the average time it took for the channel to recover to a given value. We next obtained a curve of *cis* Ca^{2+} versus *trans* Ca^{2+} (to obtain the same fractional current) divided by the time necessary to reach a steady recovery response (Fig. 5 *c*). The best fitted theoretical curve had a slope of 2×10^{-5} s (Fig. 5 *c*), which represents the Ca^{2+} flux coefficient (t_{Ca}) through the $PC2_{hst}$ channel. A summary of conclusions obtained from these calculations, including the Ca^{2+} permeability at physiological Ca^{2+} gradients, is given in the Discussion (see below).

Phenomenological model

The encompassed results were explored in terms of a phenomenological model (Eq. 7) that approximated the temporal response of the $PC2_{hst}$ currents (I_m/I_{ctrl}) after addition of either EGTA or BAPTA for the various *cis* and *trans* Ca^{2+} concentrations, as

$$\frac{I_m}{I_{ctrl}} = A + Bt - Cte^{-Dt}, \tag{7}$$

where the parameters *A*, *B*, *C*, and *D* are constants, and *t* is the time after addition of the chelator. The fitting parameters are shown in Table S3. This model considered that the overall kinetics of current decay after chelation would occur due to two simultaneous processes taking place after addition of the *cis* chelator. The first contribution would be a deficit in local Ca^{2+} which, in turn, modified the Ca^{2+} bound to the regulatory sites associated with, but not intrinsic to, the $PC2_{hst}$ channel. A second contribution to this local pool is associated with an entry step feeding Ca^{2+} through the open channel. Thus, the Ca^{2+} associated with the regulatory binding sites would primarily be determined by:

1. The initial Ca^{2+} concentration (represented by *A*, relative value);
2. Ca^{2+} entry through the channel (*Bt*); and
3. Ca^{2+} retrieval from the regulatory sites as the result of the chelating reaction and diffusion (Cte^{-Dt}).

This equation best approximated all experimental data from the various conditions tested (Fig. 6, *a* and *b*).

DISCUSSION

The human placenta transfers ~30 grams of Ca^{2+} during late gestation. The mechanisms implicated in this transepithelial

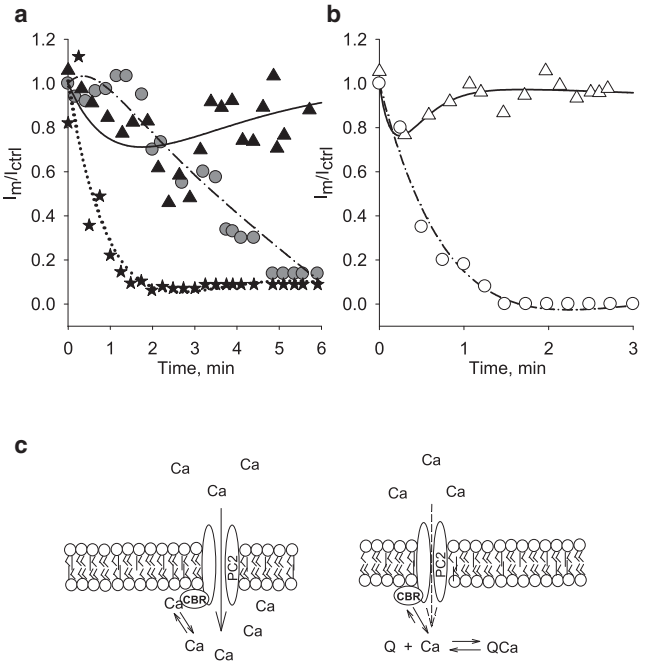

FIGURE 6 Phenomenological model. (*a*) Fitted curves obtained with the phenomenological model (Eq. 7) for EGTA additions. Experimental data were obtained after *cis* EGTA addition, for different *trans* Ca^{2+} concentrations, 1 mM, 10 μM, and 0.6 nM (*triangles*, *circles*, and *stars*, respectively). (*b*) Fitted curves obtained for BAPTA conditions and two different *trans* Ca^{2+} concentrations, 1 mM, and 10 μM (*triangles* and *circles*, respectively). The fitting parameters obtained are listed in Table S3 in the Supporting Material. (*c*) Diagram of Ca^{2+} interactions with $PC2_{hst}$. Ca^{2+} flows through the channel pore. The mobile chelating agents (*Q*) compete for a local pool of Ca^{2+} (fixed buffer) on *cis* side, contained in a microdomain accessible from the *trans* side while the channel is open. $PC2_{hst}$ channel function will depend on the Ca^{2+} level reached in the *cis* microenvironment by interaction with the Ca^{2+} binding region (*CBR*).

transport are the subject of active research (4,22,23). PC2 is implicated in Ca^{2+} transport in Ca^{2+} handling epithelia including the kidney and the placenta. The first functional characterization of PC2 as a Ca^{2+}-permeable nonselective cation channel was made in hST from term placenta (7). Little is known, however, as to how Ca^{2+} controls PC2 function in this epithelium. Herein, we explored the regulation by $Ca^{2+}$of $PC2_{hst}$ from apical hST membranes we have previously characterized (7). We observed that a decrease in free *cis* Ca^{2+} to subnanomolar levels obtained with either EGTA or BAPTA extensively inhibited $PC2_{hst}$ channel function. Current decay after chelation with EGTA (symmetrical 10 μM Ca^{2+}) was slower and incomplete, compared with the inhibition observed with BAPTA.

Surprisingly, similar experiments conducted with $PC2_{iv}$ showed no changes in channel activity. This discrepancy suggests that the $PC2_{hst}$ channel complex is somewhat different from the isolated protein. A difference may relate to a channel complex in the hST preparation that contains other channel subunits that are absent in the in vitro material and/or themselves regulated by Ca^{2+}. TRP channel monomers other than PC2 have been reported to interact with PC2 (24). In such a case, the heterocomplex may respond to Ca^{2+} in a distinct manner not observed for the isolated protein. We previously have compared PC2 channel function from various preparations in membranes, including the hST, with isolated protein from PC2-overexpressing Sf9 cells (7) and renal epithelial cells (25,26) as well as the in vitro translated material (7,24,27). We thereby identified a number of intrinsic features of the channel that were confirmed throughout. All these PC2 preparations essentially show the same functional channel properties. TRPC1-PC2 heterocomplexes, for example, show distinct structural-functional properties, including overall and subconductance states, as well as pH and amiloride sensitivity. Thus, it is likely that the $PC2_{hst}$ channel may actually present distinct associated properties instead, which modified Ca^{2+} binding, but not its biophysical properties.

Changes in Ca^{2+} are already known to regulate PC2 (16,26), although these studies were conducted with channel preparations that may contain PC2-associated proteins as well. Ehrlich's group recently found Ca^{2+}-dependent conformational changes of the isolated carboxy terminus of PC2 (27), supporting the contention that the PC2 channel has Ca^{2+}-interacting domains. It is presently unknown as to whether this phenomenon conveys any functional properties to the complete channel complex. Our contemporary observations suggest that the *cis* Ca^{2+} regulatory sites were not intrinsic to the channel, but instead related to associated proteins. The actual Ca^{2+}-binding linkers implicated in this regulation remain to be identified. Nonetheless, we have preliminary evidence that the $PC2_{iv}$ channel can be made responsive to Ca^{2+} in a manner rather similar to the $PC2_{hst}$ material, simply by adding α-actinin (M. d. R. Cantero and H. F. Cantiello, unpublished). This is in agreement with previous studies (17,28), which demonstrated a direct structural-functional interaction between PC2 and the actin-associated protein α-actinin, which binds to, and modulates $PC2_{hst}$ channel function (28). Further, F-actin severing proteins, such as gelsolin, also regulate $PC2_{hst}$ in a Ca^{2+}-dependent manner (17). Thus, cytoskeletal structures present in apical hST vesicles may provide a kinetic compartment, forming a Ca^{2+}-dependent microdomain that controls PC2 channel function.

Number of regulatory Ca^{2+} binding sites associated with the PC2 channel

The reversal from inhibition by titration with Ca^{2+} after chelation followed a well-approximated Hill equation. The n_H obtained in the presence of either chelator, was consistent with at least four Ca^{2+} regulatory sites, with apparent K_D in the range of 1–5 nM. It is important to mention that although the K_D and n_H in Eq. 2 are mathematically possible, Hill assumptions are not physically possible except for the condition in which $n = 1$ (29). Thus,

evaluation of the intrinsic dissociation constant for the first site, K_S, was necessary to better understand the potential effect of Ca^{2+} at physiological levels. A strong positive cooperativity between the Ca^{2+} binding sites was observed by the nonlinear curves in the Scatchard and Hanes plots, and confirmed by the large shift in R_s to values much lower than 81 (4.31 and 3.44 for EGTA and BAPTA, respectively; see Results) (18,19). Although n_H will be between the limits $1 < n_H < n$, it is also important to note that the more pronounced the positive cooperativity, the closer n_H will approach n, which is the true number of binding sites, and when cooperativity is maximal, n_H equals n. We further explored the decrease in the affinity constant for the first binding by expansion of the Hill equation, considering the interaction factors (Eq. 3). The summarized data in Table S2 clearly indicated that the first occupied site has an affinity of 105–111.6 nM, which is consistent with basal cytosolic Ca^{2+}, and an increase in affinity between 10 and 100 times for the other sites, as expected (18,19).

Differences between chelator responses

There were clear kinetic differences between the electrical responses of BAPTA and EGTA in symmetrical Ca^{2+} (10 μM). BAPTA was seven-times faster (3.6 vs. 0.4 min) than EGTA. This phenomenon could not be explained by differences in the forward rate constant (k_{on}) for either chelator, because the BAPTA k_{on} rate is a hundred times faster than that of EGTA (20). Moreover, EGTA produced a partial inhibition whereas BAPTA completely inhibited $PC2_{hst}$ channel function. Despite the fact that the experiments were conducted in a bilayer reconstitution system which may be envisioned as an entirely exchangeable infinite reservoir, the constraints of a kinetic compartment were in agreement with previous findings in cell models (30,31). The fast exocytotic response in melanotropic cells, a phenomenon coupled to voltage-gated Ca^{2+} channels, is very sensitive to mobile Ca^{2+} buffers, such that EGTA elicits a complete block of the response (31). Kits et al. (31) found that BAPTA blocked exocytosis only twice as effectively as EGTA. Using computer simulations, Kits et al. (31) demonstrated that these results could be explained neither by free diffusion nor by the binding rates of the mobile buffers, but instead that saturation of local Ca^{2+} buffers was involved. In their studies, a diffusional barrier for both Ca^{2+} and buffer molecules reduced diffusion 1000–10,000 times to generate similar local Ca^{2+} concentrations for specific concentrations of EGTA and BAPTA. Kits et al. concluded that when the effects of a fixed buffer are taken into consideration, the experimental results are not explained by diffusion or mobile buffer properties. This is qualitatively in agreement with our findings that show that the transport coefficient (h) obtained to correct the diffusional contribution of Ca^{2+} to both chelators was unable to explain the experimental differences for either chelator. Local buffer saturation may occur due to the existence of diffusional barriers formed by a kinetic constraint to Ca^{2+} binding. Thus, the influence of mobile Ca^{2+} buffers on Ca^{2+}-dependent processes far from the site of Ca^{2+} entry may actually depend largely on submembranous compartmentalization (31).

Other studies (32,33) similarly showed that it is not the difference in binding rate but rather the difference in affinity constants that is relevant in the Ca^{2+} chelation by EGTA and BAPTA. In general, fixed buffers will slow down and prolong the occurrence of Ca^{2+}-dependent processes because they contribute to initial chelating of ions but release Ca^{2+} when free levels drop, thus allowing for extended duration of the process (34). Naraghi and Neher (20) showed that fixed buffers do not affect the steady-state concentration of Ca^{2+} in the microdomain, but somewhat prolong the time course leading to the steady-state condition. Only very high levels of fixed buffer cause a drop in Ca^{2+} concentration very close to the membrane. Fixed buffers then will become dominant over mobile buffers, which results in equal effects of different concentrations of EGTA and BAPTA close to the membrane. This is particularly relevant in the context of our findings, which require kinetic constraints to slow down the response in the range of minutes, several orders-of-magnitude slower than either diffusion or binding rates.

Ca^{2+} transport through the PC2 channel

The differences in response between *cis* EGTA and BAPTA in the presence of 10 μM *trans* Ca^{2+} were twofold. On the one hand, there was a faster inhibition kinetics with BAPTA than EGTA; on the other hand, the inhibition with EGTA was incomplete, leaving a remainder channel function. This remaining activity proved to be efficient in reversing the inhibitory effect of the chelator by titration with *trans* Ca^{2+}. Failure to recover channel function by addition of *trans* Ca^{2+} after complete inhibition by *cis* BAPTA suggested that the Ca^{2+} regulatory sites were only accessible from the *cis* side, and thus inaccessible once the channel closed. Titration after (*cis*) chelator inhibition therefore depended on both the chelator and the concentration of *trans* Ca^{2+} at the beginning of the experiment. This was confirmed by the second set of experiments in which *cis* Ca^{2+} chelation was conducted at different initial *trans* Ca^{2+} concentrations. In the presence of higher *trans* Ca^{2+} (1 mM), for example, *cis* EGTA only elicited a transient and lower inhibition. Similarly, *cis* BAPTA inhibition in higher initial *trans* Ca^{2+} (1 mM) was also transient, resembling the EGTA effect at lower *trans* Ca^{2+}. This is consistent with a scenario whereby PC2-mediated Ca^{2+} fed through the channel into the cytoplasmic domain would help maintain channel function. This contribution could be quantified from the inverse relationship observed between $t_{1/2}$ of the activating response, and the external Ca^{2+} concentration,

such that the higher the Ca^{2+} gradient, the faster the saturation of the *cis* Ca^{2+} regulatory sites.

From the *cis*-to-*trans* Ca^{2+} response ratio, we obtained a flux coefficient (t_{Ca}) of 2×10^{-5} s, reflecting the average time it took for Ca^{2+} to pass through the pore (*trans*→*cis*), then access and activate the *cis*-located Ca^{2+} regulatory binding sites. The t_{Ca} also provided a tool for estimating the Ca^{2+} flux (J_{Ca}) through the $PC2_{hst}$ channel pore at physiologically relevant Ca^{2+} concentrations. To turn this value into either a meaningful J_{Ca} or current (I_{Ca}), we created a geometrical model of the channel pore, envisioned as a cylinder of area $\pi \times r^2$, and volume $\pi \times r^2 \times L$. We assumed an inner radius of the channel to be at least 5 nm, based on its cationic permeability properties (33). Other dimensions included a maximum diameter of 20 nm and total length of 10 nm, based on a 1:5 total ratio, and 10 times the protruding section of the channel (L), respectively, as we recently determined by atomic force microscopy (35). Thus, the internal volume (V_{pore}) that a given ion should travel would be between 0.079 and 1.25×10^{-17} cm^3. The theoretical Ca^{2+} permeability of the pore could then be estimated by

$$P_{Ca} = \frac{V_{pore}}{t_{Ca}}, \tag{8}$$

where P_{Ca} is the Ca^{2+} permeability coefficient in this concentration range. The calculated P_{Ca} was between 0.39 and 6.28×10^{-13} cm^3/s. Thus, J_{Ca} through $PC2_{hst}$ would then be obtained as postulated by Läuger (36) such that

$$J_{Ca} = P_{Ca}\left[\frac{za}{2\sinh(a/2)}\right]\left([Ca]_{trans}e^{\frac{a}{2}} - [Ca]_{cis}e^{-\frac{a}{2}}\right), \tag{9}$$

where $a = RTV/zF$ and V is the applied holding potential. The value obtained, J_{Ca}, in the range of 9.32×10^{-20} mol/s and 1.48×10^{-18} mol/s, would be consistent with a $PC2_{hst}$ Ca^{2+} conductance of ~0.15–2.38 pS at 1 mM external Ca^{2+}. These results were in agreement with a boundary condition obtained by calculation of the maximal Ca^{2+} permeability P_{Ca}^{max}, as estimated by Läuger (36),

$$P_{Ca}^{max} = 2\pi r_o D_{Ca}, \tag{10}$$

where r_o is a hemispherical surface parameter that represents an effective capture radius. Considering an r_o = 0.1 nm (36) and the Ca^{2+} diffusion coefficient of 660 $\mu m^2/s$ (20), the P_{Ca}^{max} and J_{Ca}^{max} would be 4.15×10^{-13} cm^3/s and 3.92×10^{-15} mol s^{-1}, respectively, giving a maximal conductance of 6.30 pS. This value represents a very high Ca^{2+} transport rate compared to most Ca^{2+}-permeable channels under the imposed electrochemical conditions (37). In addition, we validated the Ca^{2+} transport data by direct electrodiffusional experiments (see the Supporting Material). We obtained current-to-voltage (I/V) relationships of $PC2_{hst}$ single channel currents under biionic conditions with a *cis*→*trans* K^+ gradient and a high *trans* Ca^{2+} concentration (90 mM), such that Ca^{2+} currents from *trans* to *cis* could be determined (see Fig. S2). The I/V data obtained were well fitted with both the Goldman-Hodgkin-Katz equation and an absolute rate theory model containing two internal Ca^{2+} binding sites within the pore of the channel (38). The K_D values calculated were used to obtain a Michaelis-Menten-type g_{PC2} versus $Ca^{2+}{}_{trans}$ curves. A Ca^{2+} single channel conductance in the range of 0.12–1.33 pS was obtained for 1 mM *trans* Ca^{2+}, in close agreement with 0.15–2.38 pS, obtained from the Ca^{2+} transfer data.

Size of the Ca^{2+} microdomain

From the J_{Ca}^{max} range obtained under our experimental conditions, and the average time it took for Ca^{2+} to attain a given activation response, say an increase in channel activity from 20 to 80%, it could be estimated that the delivery of ~5×10^{-17} moles of Ca^{2+} to the *cis* side would be required. This estimation suggests a local volume associated with the kinetic differences between EGTA and BAPTA of ~8–10 nL, which reflects a large microdomain associated with the $PC2_{hst}$ channel. Considering the geometry and expected diffusional properties of the *cis* chamber, it is expected that this microdomain is most likely associated with the cytoskeletal network linked to the channel in the hST apical vesicles (as seen in Montalbetti et al. (17)).

Phenomenological model

The results in this report were best followed by a phenomenological model (Eq. 7) describing the kinetic changes in $PC2_{hst}$ channel activity as a function of Ca^{2+}, and entails, as indicated above, the presence of a local pool of Ca^{2+} (microdomain) buffering Ca^{2+} regulatory sites associated with the cytoplasmic side of the $PC2_{hst}$ channel, whose saturation would depend on two contributing processes: the high affinity binding sites of an associated protein and the rate of Ca^{2+} delivered through the channel. The first contribution is evidenced as Ca^{2+} is depleted by addition of the chelating agent. The other (compensating) contribution lies in the Ca^{2+} entry through the channel pore. This is described as a linear parameter related to the electrochemical Ca^{2+} gradient. The parameters obtained using this model (see Table S3) could be interpreted as the contribution of both Ca^{2+} input and output to and from the microdomain near the channel, respectively.

Competition between Ca^{2+} influx through the channel, and Ca^{2+} chelation by either mobile buffer, determines the degree of depletion (or not) of the microdomain, and therefore the effected system, $PC2_{hst}$ function. Thus, in the presence of BAPTA and 10 μM *cis* Ca^{2+}, the contribution of the exponential term is larger, compared to that

obtained in the presence of EGTA. This indicates a greater depletion of the microdomain in the presence of BAPTA. In the presence of BAPTA and 1 mM *trans* Ca^{2+}, however, the absence of channel inhibition would reflect the larger contribution of Ca^{2+} entry through the channel, from the *trans* side. Moreover, in the presence of either chelator and 1 mM *trans* Ca^{2+}, the linear term of Eq. 3 representing Ca^{2+} influx through the channel is greater than in the presence of lower concentrations (0.6 nM and 10 μM). Thus, Ca^{2+} transport (*trans* → *cis*) through the channel largely contributes to maintain the channel open (Fig. 6 *c*).

CONCLUSIONS

The data in this report indicate that a local cytoplasmic Ca^{2+} binding region associated with PC2 (*CBR*, Fig. 6 *c*) regulates its channel activity in the hST preparation. This Ca^{2+} regulatory region is absent in the isolated protein, and represents a Ca^{2+} binding protein(s) that associate with, and confer Ca^{2+}-dependence to, the channel. Ca^{2+} feed through the channel would replete and control this Ca^{2+} microdomain. The data suggest a high intrinsic Ca^{2+} permeability by PC2.

SUPPORTING MATERIAL

Materials, methods, two figures, three tables, and reference (39) are available at http://www.biophysj.org/biophysj/supplemental/S0006-3495(13)00677-2.

The authors thank Dr. Patricia Bonazzola for unconditional support and encouragement, and acknowledge Dr. Fernando Marengo (Facultad de Ciencias Exactas y Naturales, Universidad de Buenos Aires), for providing BAPTA.

M.d.R.C. and H.F.C. are members of the Consejo Nacional de Investigaciones Científicas y Técnicas, Argentina.

REFERENCES

1. Givens, M. H., and I. C. Macy. 1933. The chemical composition of the human fetus. *J. Biol. Chem.* 102:7–17.
2. Salle, B. L., J. Senterre, …, G. Putet. 1987. Vitamin D metabolism in preterm infants. *Biol. Neonate.* 52(*Suppl 1*):119–130.
3. Brunette, M. G. 1988. Calcium transport through the placenta. *Can. J. Physiol. Pharmacol.* 66:1261–1269.
4. Belkacemi, L., I. Bédard, …, J. Lafond. 2005. Calcium channels, transporters and exchangers in placenta: a review. *Cell Calcium.* 37:1–8.
5. Hoenderop, J. G. J., B. Nilius, and R. J. M. Bindels. 2005. Calcium absorption across epithelia. *Physiol. Rev.* 85:373–422.
6. Hoenderop, J. G., R. Vennekens, …, B. Nilius. 2001. Function and expression of the epithelial Ca^{2+} channel family: comparison of mammalian ECaC1 and 2. *J. Physiol.* 537:747–761.
7. González-Perrett, S., K. Kim, …, H. F. Cantiello. 2001. Polycystin-2, the protein mutated in autosomal dominant polycystic kidney disease (ADPKD), is a Ca^{2+}-permeable nonselective cation channel. *Proc. Natl. Acad. Sci. USA.* 98:1182–1187.
8. Mochizuki, T., G. Wu, …, S. Somlo. 1996. PKD2, a gene for polycystic kidney disease that encodes an integral membrane protein. *Science.* 272:1339–1342.
9. Cantiello, H. F. 2004. Regulation of calcium signaling by polycystin-2 (Review). *Am. J. Physiol. Renal Physiol.* 286:F1012–F1029.
10. Tsiokas, L. 2009. Function and regulation of TRPP2 at the plasma membrane. *Am. J. Physiol. Renal Physiol.* 297:F1–F9.
11. Zhou, J. 2009. Polycystins and primary cilia: primers for cell cycle progression (Review). *Annu. Rev. Physiol.* 71:83–113.
12. Imredy, J. P., and D. T. Yue. 1994. Mechanism of Ca^{2+}-sensitive inactivation of L-type Ca^{2+} channels. *Neuron.* 12:1301–1318.
13. Li, Q., Y. Liu, …, X. Z. Chen. 2002. The calcium-binding EF-hand in polycystin-L is not a domain for channel activation and ensuing inactivation. *FEBS Lett.* 516:270–278.
14. Nilius, B., F. Weidema, …, R. J. Bindels. 2003. The carboxyl terminus of the epithelial Ca^{2+} channel ECaC1 is involved in Ca^{2+}-dependent inactivation. *Pflugers Arch.* 445:584–588.
15. Vassilev, P. M., L. Guo, …, J. Zhou. 2001. Polycystin-2 is a novel cation channel implicated in defective intracellular Ca^{2+} homeostasis in polycystic kidney disease. *Biochem. Biophys. Res. Commun.* 282:341–350.
16. Cai, Y., G. Anyatonwu, …, S. Somlo. 2004. Calcium dependence of polycystin-2 channel activity is modulated by phosphorylation at Ser^{812}. *J. Biol. Chem.* 279:19987–19995.
17. Montalbetti, N., Q. Li, …, H. F. Cantiello. 2005. Cytoskeletal regulation of calcium-permeable cation channels in the human syncytiotrophoblast: role of gelsolin. *J. Physiol.* 566:309–325.
18. Segel, I. H. 1975. Enzyme kinetics. *In* Behavior and Analysis of Rapid Equilibrium and Steady State Enzyme Systems. Wiley-Interscience, New York.
19. Bisswanger, H. 2008. Enzyme kinetics. *In* Principles and Methods, 2nd Ed. Wiley-VCH, Weinheim, Germany.
20. Naraghi, M., and E. Neher. 1997. Linearized buffered Ca^{2+} diffusion in microdomains and its implications for calculation of $[Ca^{2+}]$ at the mouth of a calcium channel. *J. Neurosci.* 17:6961–6973.
21. Klingauf, J., and E. Neher. 1997. Modeling buffered Ca^{2+} diffusion near the membrane: implications for secretion in neuroendocrine cells. *Biophys. J.* 72:674–690.
22. Moreau, R., A. Hamel, …, J. Lafond. 2002. Expression of calcium channels along the differentiation of cultured trophoblast cells from human term placenta. *Biol. Reprod.* 67:1473–1479.
23. Bernucci, L., M. Henríquez, …, G. Riquelme. 2006. Diverse calcium channel types are present in the human placental syncytiotrophoblast basal membrane. *Placenta.* 27:1082–1095.
24. Zhang, P., Y. Luo, …, H. F. Cantiello. 2009. The multimeric structure of polycystin-2 (TRPP2): structural-functional correlates of homo- and hetero-multimers with TRPC1. *Hum. Mol. Genet.* 18:1238–1251.
25. Li, Q., X. Q. Dai, …, X.-Z. Chen. 2004. A modified mammalian tandem affinity purification procedure to prepare functional polycystin-2 channel. *FEBS Lett.* 576:231–236.
26. Chen, X. Z., Y. Segal, …, J. Zhou. 2001. Transport function of the naturally occurring pathogenic polycystin-2 mutant, R742X. *Biochem. Biophys. Res. Commun.* 282:1251–1256.
27. Ćelić, A. S., E. T. Petri, …, T. J. Boggon. 2012. Calcium-induced conformational changes in C-terminal tail of polycystin-2 are necessary for channel gating. *J. Biol. Chem.* 287:17232–17240.
28. Li, Q., N. Montalbetti, …, X. Z. Chen. 2005. Alpha-actinin associates with polycystin-2 and regulates its channel activity. *Hum. Mol. Genet.* 14:1587–1603.
29. Weiss, J. N. 1997. The Hill equation revisited: uses and misuses. *FASEB J.* 11:835–841.
30. Mansvelder, H. D., and K. S. Kits. 1998. The relation of exocytosis and rapid endocytosis to calcium entry evoked by short repetitive depolarizing pulses in rat melanotropic cells. *J. Neurosci.* 18:81–92.

31. Kits, K. S., T. A. de Vlieger, …, H. D. Mansvelder. 1999. Diffusion barriers limit the effect of mobile calcium buffers on exocytosis of large dense cored vesicles. *Biophys. J.* 76:1693–1705.

32. Seward, E. P., and M. C. Nowycky. 1996. Kinetics of stimulus-coupled secretion in dialyzed bovine chromaffin cells in response to trains of depolarizing pulses. *J. Neurosci.* 16:553–562.

33. Nowycky, M. C., and M. J. Pinter. 1993. Time courses of calcium and calcium-bound buffers following calcium influx in a model cell. *Biophys. J.* 64:77–91.

34. Sala, F., and A. Hernández-Cruz. 1990. Calcium diffusion modeling in a spherical neuron. Relevance of buffering properties. *Biophys. J.* 57:313–324.

35. Anyatonwu, G. I., and B. E. Ehrlich. 2005. Organic cation permeation through the channel formed by polycystin-2. *J. Biol. Chem.* 280:29488–29493.

36. Läuger, P. 1976. Diffusion-limited ion flow through pores. *Biochim. Biophys. Acta.* 455:493–509.

37. Demuro, A., and I. Parker. 2006. Imaging single-channel calcium microdomains. *Cell Calcium.* 40:413–422.

38. Cantero, M. R., and H. F. Cantiello. 2011. Effect of lithium on the electrical properties of polycystin-2 (TRPP2). *Eur. Biophys. J.* 40:1029–1042.

39. Hille, B., and W. Schwarz. 1978. Potassium channels as multi-ion single-file pores. *J. Gen. Physiol.* 72:409–442.

Supporting Material

"Calcium Transport and Local Pool Regulate Polycystin-2 (TRPP2) Function in Human Syncytiotrophoblast". Cantero MR and Cantiello HF.

Materials and Methods

Human placenta membrane preparation. Apical hST plasma membranes from term human placenta were obtained as previously described (1). Briefly, normal placenta from vaginal deliveries were obtained and immediately processed. The villous tissue was fragmented, washed with ice-cold unbuffered NaCl saline (150 mM), and minced into small pieces. The fragmented tissue was processed, filtered and centrifuged, as previously reported (1). The final pellet was resuspended in a buffer solution containing (in mM): HEPES 10, sucrose 250, and KCl 20, adjusted to pH 7.4, which was aliquoted and stored frozen until the time of the experiment. Apical hST enrichment usually was higher than 26-fold.

Preparation of in vitro translated PC2. In vitro translated PC2 ($PC2_{iv}$) was prepared as previously reported (1). The plasmid pGEM-PKD2 encoding PC2, was *in vitro* transcribed and translated with a reticulocyte lysate system TnT T7 (Promega) by incubation of plasmid DNA (1 μg) and 50 μl of the reaction mixture for 90 min at 30°C. The $PC2_{iv}$ was introduced by dialysis into liposomes as previously reported (1).

Ion channel reconstitution. PC2 containing vesicles were incorporated into lipid bilayers of a reconstitution system. The lipid mixture was a 7:3 ratio of POPC and POPE (20-25 mg/ml, Avanti Polar Lipids, Birmingham, AL) in n-decane. Unless otherwise stated, the *cis* chamber contained a solution of: KCl 150 mM, $CaCl_2$ 10 μM, HEPES 10 mM, at pH 7.40. The *trans* side contained a similar solution with lower KCl (15 mM), to create a KCl chemical gradient. $PC2_{hst}$ was identified as previously reported (1), by a large conductance (~170 pS), K^+-conducting channel, which was inhibited by *trans* (external) amiloride, and *cis* (cytoplasmic side of PC2) anti-PC2 antibody, properties that also ensured its orientation in the reconstituted membrane (1).

Reagents and Ca^{2+} chelation. Unless otherwise stated, reagents were obtained from Sigma-Aldrich (St. Louis, MO). Ethylene-bis(oxyethylenenitrilo)tetraacetic acid (EGTA, 100 mM) was dissolved in NaOH and titrated with HCl to reach pH 7.1 in the stock solution, before use. Ethylenedioxybis(o-phenylenenitrilo)tetraacetic acid (BAPTA, 250 mM) was dissolved in dimethylsulfoxide (DMSO). The concentrated reagents EGTA and BAPTA (16 μl and 8 μl, respectively) were diluted in either *cis* (1600 μl) or *trans* (1000 μl) chambers, buffered at pH 7.4 to reach a final concentration of 1 mM and 2 mM, respectively (see Results). Neither the addition of either chelator, nor vehicle alone to the chamber solution elicited any change in the final pH, which was kept at 7.4 with 10 mM HEPES. Calculations were corroborated by the free on-line site http://www.stanford.edu/~cpatton/CaEGTA-NIST.htm. The final free Ca^{2+} concentration was estimated to be either 0.6 nM or 0.8 nM (pH ~7.4) in the presence of EGTA or BAPTA, respectively. Whenever indicated, $CaCl_2$ was added to the chamber, from stock solutions ranging from 1 mM to 1 M to the final concentrations indicated in the Results section. In all cases, the added Ca^{2+} chelator was kept throughout the entire experiment.

Data acquisition and analysis. Electrical signals were obtained with a PC501A patch clamp amplifier (Warner Instruments, Hamden, CT) with a 10 Gohm feedback resistor. Output (voltage) signals were

low-pass filtered at 700 Hz (3 dB) with an eight pole, Bessel type filter (Frequency Devices, Haverhill, MA). Signals were displayed in an oscilloscope and acquired using pCLAMP 6.0.2. Single channel current tracings were further filtered for display purposes only. Unless otherwise stated, pCLAMP Version 10.0 (Axon Instruments, Foster City, CA) was used for data analysis and Sigmaplot Version 11.0 (Jandel Scientific, Corte Madera, CA) for statistical analysis and graphics. Unless otherwise stated, all tracings shown in this study were obtained at holding potentials between 40 and 60 mV. PC2 channel identification was conducted as previously reported (1). Statistical significance was obtained by unpaired Student's test comparison of sample groups of similar size, and accepted at $p < 0.05$. Average data values were expressed as the mean ± SEM (N) under each condition, where n represents the total number of experiments analyzed.

Results

Diffusional limitation corrections. The 7 to 1 relationship between the $t_{1/2}$ obtained in the presence of 10 μM Ca^{2+} and either EGTA or BAPTA addition, could be explained neither by the binding interaction itself nor by the forward rate constants of the chelators (2). Thus, we explored the possibility that a diffusional limitation of the chelators could exist, limiting their access to Ca^{2+} binding sites. To this end, we corrected the experimental recovery curves by the transport coefficient (h) as described in (3), representing the existence of a diffusional layer between the channel and the bulk Ca^{2+} present, which would have distinct diffusive properties for either chelator. We plotted I_m/I_{max} *vs.* time, after Ca^{2+} addition to the *cis* chamber following inhibition by either EGTA or BAPTA (Fig. S1a), respectively. The h values obtained (Fig. S1b) were not statistically different from each other (see Results Section in the main text, $p > 0.05$), indicating that the two chelators did not display any relevant diffusional differences. The corrected $K_D s$ values obtained (4.70 ± 0.02 nM and 1.26 ± 0.03 nM, in the presence of EGTA and BAPTA addition, respectively) fell within the experimental error, such that the diffusional contribution would be negligible for either chelator.

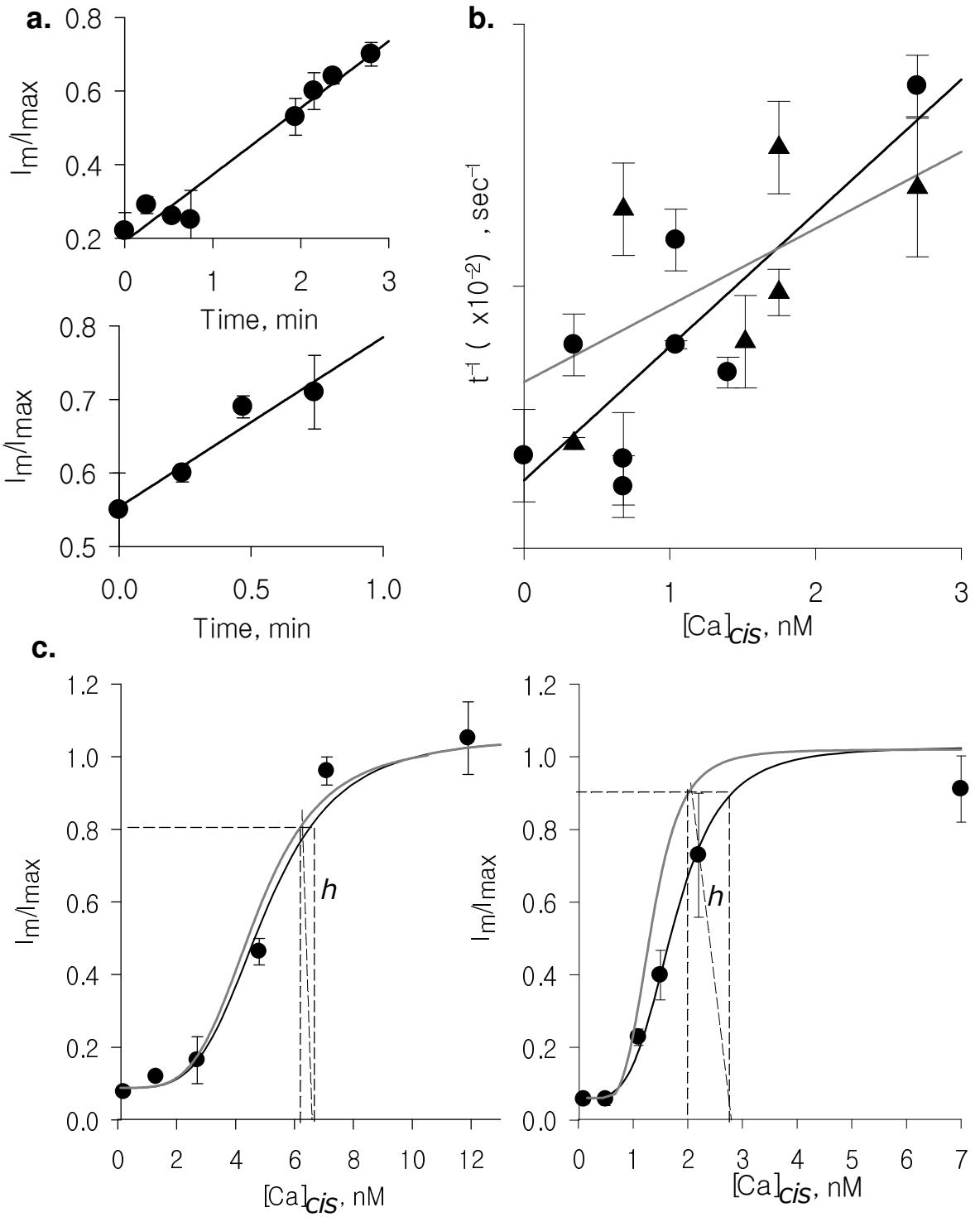

Fig. S1. ***Diffusional contribution to the K_D constants. a.*** *Representative I_m / I_{max} as a function of a given cis Ca^{2+}, after inhibition with either EGTA (upper panel, N = 4) or BAPTA (lower panel, N = 3). The solid lines represent the best fitted linear correlation. Experimental data (circles) are expressed as mean ± SEM.* ***b.*** *The slopes obtained for several Ca^{2+} concentrations (as in* ***a.****) were plotted against [Ca^{2+}] after addition of either EGTA (circles, N = 7) or BAPTA 2 mM cis (triangles, and N = 3).* ***c.*** *The Hill type curve was corrected for the diffusive process (3) for the EGTA (Left) and BAPTA (Right) curves. Experimental data plotted are the mean ± SEM.*

Modelling of $PC2_{iv}$ under various Ca^{2+} conditions using the 2S3B energy model. The single channel currents through PC2 were fitted with a 2S3B model, representing a minimal channel model that allows multiple occupancy and saturation (4). The model included six energy parameters: three peak energies (G_{12}, G_{23} and G_{34}), two well energies (G_2 and G_3), and three electrical distances (d_1 to d_3), that represent the fraction of the electric field energetically separating peaks and wells, with the requirement that the sum $2(d_1+d_2+d_3)$ equals one. An interaction parameter, $A = F_{out}/F_{in}$, was also included to represent ion-ion interactions, where F_{in} and F_{out} are the repulsion factors inside and out the channel, respectively, whenever the channel is occupied by ions. I/V experimental data were fitted, for high activity range (4, 5) with Eq. S1:

$$I = zFQ\,exp\left(-G_{23}+G_3+G_2\right)A\left\{\frac{exp\left[\left(d_2+2d_1\right)V\right]}{\left[S^+\right]_{trans}}-\frac{exp\left[-\left(d_2+2d_3\right)V\right]}{\left[S^+\right]_{cis}}\right\} \qquad \text{Eq. (S1)}$$

where d_1, d_2 and d_3 are the electrical distances, G_{23}, G_3 and G_2 are the energy of peak and valleys respectively.

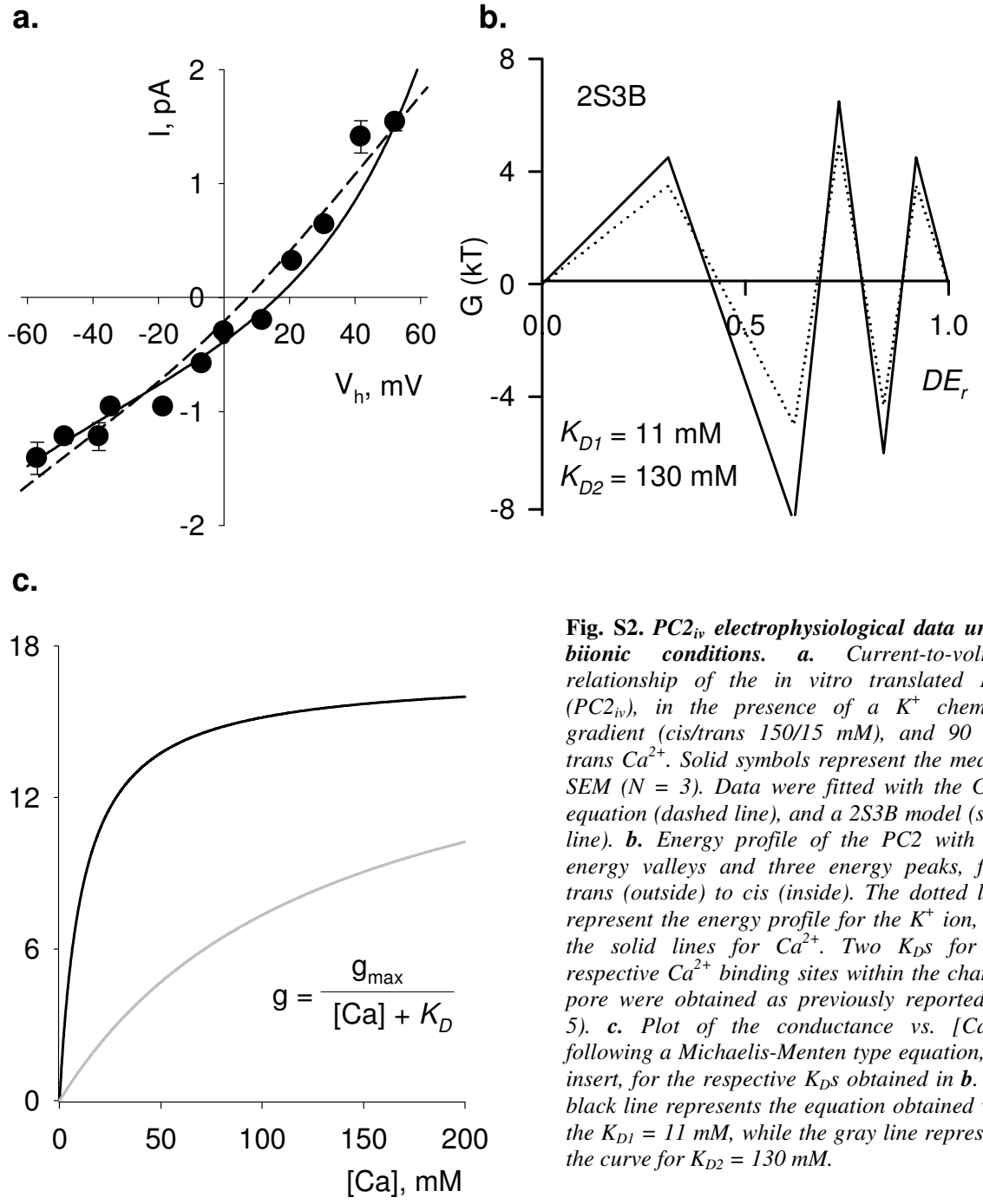

Fig. S2. ***$PC2_{iv}$ electrophysiological data under biionic conditions.*** ***a.*** *Current-to-voltage relationship of the in vitro translated PC2 ($PC2_{iv}$), in the presence of a K^+ chemical gradient (cis/trans 150/15 mM), and 90 mM trans Ca^{2+}. Solid symbols represent the mean ± SEM (N = 3). Data were fitted with the GHK equation (dashed line), and a 2S3B model (solid line).* ***b.*** *Energy profile of the PC2 with two energy valleys and three energy peaks, from trans (outside) to cis (inside). The dotted lines represent the energy profile for the K^+ ion, and the solid lines for Ca^{2+}. Two K_Ds for the respective Ca^{2+} binding sites within the channel pore were obtained as previously reported (4, 5).* ***c.*** *Plot of the conductance vs. $[Ca^{2+}]$, following a Michaelis-Menten type equation, see insert, for the respective K_Ds obtained in* ***b****. The black line represents the equation obtained with the K_{D1} = 11 mM, while the gray line represents the curve for K_{D2} = 130 mM.*

Table S1. *NP_o obtained for $PC2_{iv}$ under various Ca^{2+} gradients*

Condition $[Ca^{2+}]_{cis}/[Ca^{2+}]_{trans}$	NP_o	SE (N = 3)
10 μM / 10 μM*	0.93	0.01
0.6 nM / 0.6 nM	0.94	0.02
0.6 nM / 10 μM	0.94	0.04
0.6 nM / 50 mM	0.90	0.04

*Control condition

Table S1 Legend. The Table summarizes the NP_o obtained for the $PC2_{iv}$ protein under various Ca^{2+} gradients showing the lack of response to high Ca^{2+} in the *trans* compartment.

Table S2. *Affinity factors of expanded Hill equation*.

	EGTA	**BAPTA**
K_S, *nM*	111.6 ± 6.92	105.0 ± 6.35
a	0.1190 ± 0.0024	0.0421 ± 0.0004
b	0.1289 ± 0.0089	0.0689 ± 0.0054
c	0.1603 ± 0.0205	0.2095 ± 0.0323
K_D ($= a^3b^2cK_s^4$), *nM*	5.14	1.73

Table S2 Legend. The Table summarizes the affinity factors obtained with Eq. (3) from dose-response recovery curves after inhibition with either EGTA (N = 7), or BAPTA (N = 5).

Table S3. *Phenomenological model parameters.*

Ca_{trans}	EGTA				
	A	*B*	*C*	*D*	*r*
0.6 nM	1.00 ± 0.08	-0.11 ± 0.08	1.05 ± 0.18	0.55 ± 0.07	0.93 ± 0.10
10 μM	1.00 ± 0.13	-0.15 ± 0.02	-0.36 ± 0.10	1.12 ± 0.55	0.96 ± 0.10
1 mM	1.00 ± 0.17	0.03 ± 0.06	0.45 ± 0.43	0.57 ± 0.45	0.55 ± 0.30
	BAPTA				
	A	*B*	*C*	*D*	*r*
10 μM	1.00 ± 0.05	-0.11 ± 0.01	1.16 ± 0.13	0.53 ± 0.04	0.97 ± 0.07
1 mM	1.00 ± 0.05	0.01 ± 0.02	2.65 ± 1.20	4.19 ± 1.15	0.82 ± 0.05

Table S3 Legend. The Table summarizes the parameters obtained from fitting the phenomenological model equation to experimental data under the various conditions indicated in the Table. Parameters *B*, *C*, and *D* are expressed in min^{-1}, while parameter *A* and regression coefficient "*r*" are dimensionless.

Supporting References

1. González-Perrett, S., K. Kim, C. Ibarra, A. E. Damiano, E. Zotta, M. Batelli, P. C. Harris, I. L. Reisin, M. A. Arnaout, and H. F. Cantiello. 2001. Polycystin-2, the protein mutated in autosomal dominant polycystic kidney disease (ADPKD), is a Ca^{2+}-permeable nonselective cation channel. Proc. Natl. Acad. Sci. USA 98:1182-1187.

2. Naraghi, M., and E. Neher. 1997. Linearized buffered Ca^{2+} diffusion in microdomains and its implications for calculation of $[Ca^{2+}]$ at the mouth of a calcium channel. J. Neurosci. 17:6961-6973.

3. Bisswanger, H. 2008. *Enzyme Kinetics. Principles and Methods*. 2nd Ed. Wiley-VCH, Weinheim.

4. Hille, B., and W. Schwarz. 1978. Potassium channels as multi-ion single-file pores. J. Gen. Physiol. 72:409-442.

5. Cantero, M. R., and H. F. Cantiello. 2011. Effect of lithium on the electrical properties of polycystin-2 (TRPP2). Eur. Biophys. J. 40:1029-1042.